

Inelastic light scattering from a dielectric sphere with a time-varying radius

E. Panagiotidis,^{1,2} E. Almpanis^{1,2,*}, N. Papanikolaou², and N. Stefanou¹

¹*Section of Condensed Matter Physics, National and Kapodistrian University of Athens, Panepistimioupolis, GR-157 84 Athens, Greece*

²*Institute of Nanoscience and Nanotechnology, NCSR “Demokritos,” Patriarchou Gregoriou and Neapoleos Street, Agia Paraskevi, GR-153 10 Athens, Greece*



(Received 31 December 2021; revised 28 February 2022; accepted 13 July 2022; published 27 July 2022)

This work reports on light scattering by a homogeneous dielectric sphere with a periodically time-varying radius. The off-shell inelastic scattering T matrix, which describes the dynamically changing particle, is evaluated using the Floquet method, and some remarkable phenomena, emerging in the strong- and weak-coupling regimes, are discussed. In particular, the limits of validity of the approximate quasistatic solution are established through comparison with the results of fully dynamic calculations, and the scattering in the strong-coupling regime is analyzed in terms of the general behavior of parametrically driven oscillators. Additionally, the influence of damping of the sphere vibrations on the optical spectra is also investigated.

DOI: [10.1103/PhysRevA.106.013524](https://doi.org/10.1103/PhysRevA.106.013524)

I. INTRODUCTION

Electromagnetic (EM) wave propagation in time-varying environments constitutes a very broad class of research that involves a plethora of individual problems [1]. Morgenthaler, in his pioneering works during the 1950s, dealt with monochromatic waves in a medium with changing phase velocity [2], while many other various aspects of EM wave propagation in time-varying media were studied by other groups [3–7]. From one point of view, time can be considered an extra degree of freedom to mold light propagation and control light-matter interaction. In this respect, media modulated in both time and space offer additional possibilities to control the optical response. Especially, with the emergence of time-periodic, so-called time-Floquet, photonic crystals [8–13], the field gained renewed interest.

For applications operating in the visible and near-infrared part of the spectrum, dynamic control of the medium permittivity is possible through elastic or spin waves. For instance, time modulation of optical cavities using phonons and magnons has been demonstrated in the frame of *cavity optomechanics* [14–16] and *cavity optomagnonics* [17–20], respectively, and combinations with other fields such as *cavity magnomechanics* [21], *electromechanics* [22], and *electro-optomechanics* [23]. A common platform for combining optics with dynamic excitations of other wave fields is based on whispering-gallery-mode (WGM) resonators since they strongly confine the EM field in high-finesse resonances, while they can be easily realized and experimentally probed using Brillouin light scattering (BLS) spectroscopy.

A few examples of works on WGM optomechanical cavities can be found in Refs. [24–28], while respective realizations of optomagnonic WGM resonators can be found in Refs. [29–32]. However, optical WGM resonators exhibit

a large modal volume, which translates to a weaker optomechanical and optomagnonic coupling compared to nano- and micronsized Mie scatterers. Therefore, to achieve stronger coupling in optomechanics (optomagnonics), efforts have been devoted to designing resonators of smaller size that exhibit optical Mie resonances [33–35] (Ref. [36]).

Gantzounis *et al.* [33] studied the interaction between optical Mie modes and a breathing mode of vibration in a (sub)micron-sized dielectric sphere, in the framework of the adiabatic quasistatic approximation. This approximation is valid for vibration frequencies much smaller than the photon decay rate; however, a fully dynamic approach is required to go beyond this limit. For this purpose, in the present work we develop a time-Floquet method for homogeneous spherical particles with a time-varying radius (breathing vibration). This method calculates the spherical-wave expansion coefficients of the elastically and inelastically scattered beams generated by an incoming wave. In this respect, energy transfer to the inelastically scattered light beams, mediated by the vibration, is accurately described. Our rigorous calculations reveal the occurrence of many interesting phenomena associated with inelastic light scattering from a vibrating particle and elucidate the underlying physical mechanisms. On the other hand, the time-Floquet method can easily be generalized to include temporal variation of the permittivity, as demonstrated in a previous work [37], or dynamic variation of the magnetization, but most importantly, it can readily be implemented in our layer-multiple-scattering computational methodology [38], which can be used for designing, e.g., nonreciprocal metamaterials and metasurfaces.

The rest of this paper is organized as follows: In Sec. II we develop a time-Floquet method for light scattering from a spherical particle with a periodically time-varying radius. In Sec. III we demonstrate the applicability of the method for a specific case of a vibrating microparticle and discuss some interesting effects emerging from inelastic light scattering in

*ealmpanis@gmail.com

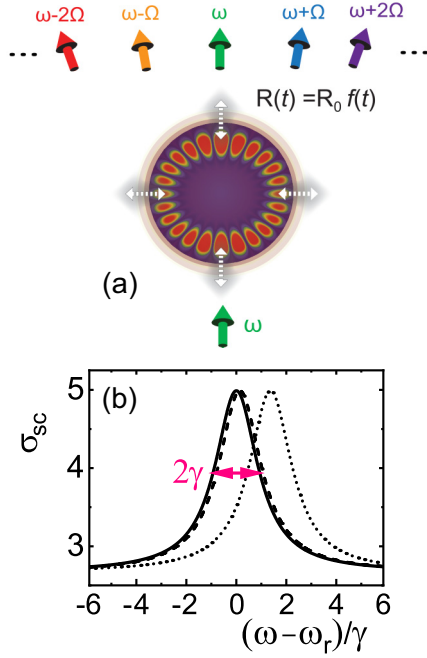


FIG. 1. (a) Graphical representation of the system under study. A silicon microparticle of radius $R = R_0$ vibrates in a breathing mode, so that $R(t) = R_0[1 + \eta \cos(\Omega t)]$. Linearly polarized monochromatic light of angular frequency ω , scattered by the particle, generates outgoing beams at frequencies $\omega, \omega \pm \Omega, \omega \pm 2\Omega, \dots$ (b) Scattering cross section of the static sphere of radius R_0 , about the first-order TE $_{\ell=12}$ Mie resonance (solid line). The scattering cross-section spectra for different radii of the sphere, $R = R_0(1 - \eta)$ for $\eta = 10^{-10}$ (dashed line) and $\eta = 10^{-9}$ (dotted line), are also displayed. The electric-field-intensity profile at the resonance frequency, in a plane that cuts the center of the sphere and is perpendicular to the polarization direction of the incident light, is depicted in (a).

different regimes of vibration frequencies and amplitudes. Finally, in Sec. IV we summarize our main findings.

II. SCATTERING BY A PARTICLE WITH A PERIODICALLY VARYING RADIUS

In the present work we are concerned with light scattering by a spherical particle of relative permittivity ϵ_M and permeability μ_M in a homogeneous medium with relative permittivity ϵ and permeability μ . The particle has a radius varying in time according to the equation $R = R_0 f(t)$, where $f(t)$ is a periodic function with a period $T = 2\pi/\Omega$. We assume an EM wave of angular frequency ω , with electric field component $\mathbf{E}_0(\mathbf{r}, t) = \text{Re}[\mathbf{E}_0(\mathbf{r}) \exp(-i\omega t)]$, incident on the given oscillating particle, as shown in Fig. 1(a). Such a plane wave can be expanded into regular vector spherical waves about a given origin at the center of the particle as follows [38]:

$$\mathbf{E}_0(\mathbf{r}) = \sum_{\ell=1}^{\infty} \sum_{m=-\ell}^{\ell} \left[\frac{i}{k} a_{E\ell m}^0 \nabla \times j_{\ell}(kr) \mathbf{X}_{\ell m}(\hat{\mathbf{r}}) + a_{H\ell m}^0 j_{\ell}(kr) \mathbf{X}_{\ell m}(\hat{\mathbf{r}}) \right], \quad (1)$$

where $k = \omega \sqrt{\epsilon \mu \epsilon_0 \mu_0} = \omega \sqrt{\epsilon \mu} / c$ is the wave number (ϵ_0 and μ_0 are the vacuum permittivity and permeability, and c is the velocity of light), $a_{p\ell m}^0$ are expansion coefficients, j_{ℓ} are spherical Bessel functions, and $\mathbf{X}_{\ell m}(\hat{\mathbf{r}})$ are the vector spherical harmonics. By $P = E$ and H we denote electric [transverse magnetic (TM)] and magnetic [transverse electric (TE)] polarization, respectively, where $\ell = 1, 2, \dots$ and $m = -\ell, -\ell + 1, \dots, \ell$ are the usual angular momentum indices. We note that, in the case of a static particle [$f(t) = 1$], the field in its interior can be expanded in a similar manner as in Eq. (1), with expansion coefficients $a_{p\ell m}^M$ and replacing k with $q = \omega \sqrt{\epsilon_M \mu_M} / c$. Similarly, for the scattered field, outgoing vector spherical waves are used, with spherical Hankel functions h_{ℓ}^+ in the place of j_{ℓ} and corresponding expansion coefficients $a_{p\ell m}^+$. These are connected to $a_{p\ell m}^0$ through a diagonal and m -independent on-shell scattering T matrix as follows: $a_{p\ell m}^+ = T_{p\ell} a_{p\ell m}^0$.

A. Inelastic scattering matrix

To describe scattering by a particle with a periodically time varying radius, we use the Floquet approach and expand the EM fields into series of time-harmonic monochromatic beams with angular frequencies $\omega_n = \omega - n\Omega$, where $n = 0, \pm 1, \pm 2, \dots$. In the problem considered here, the vibration frequencies $\Omega/2\pi$ are several orders of magnitude smaller than the EM wave frequency. In particular, typical vibrational frequencies of micron-sized spheres do not exceed on the order of gigahertz, while larger spheres exhibit lower vibrational frequencies, reaching on the order of kilohertz for diameters of a few centimeters. This means that, on the one hand, the sphere radius does not vary substantially within a period of the EM field, while, on the other hand, the instantaneous velocity of the boundary [39] is negligibly small compared to the velocity of light in vacuum. Therefore, the coefficients in the spherical wave expansions of the fields can be obtained by applying the usual boundary conditions of continuity of the tangential field components at the surface of the vibrating sphere and using Fourier series expansions for the time-periodic quantities $j_{\ell}(kR_0 f(t))$, $j_{\ell}(qR_0 f(t))$, $h_{\ell}^+(kR_0 f(t))$, etc., as detailed in Appendix A [40]. We note here that this approximation is also valid for a high- Q optical resonance, such as the one discussed in Sec. III, where our results are validated under the adiabatic quasistatic approximation. Since spherical symmetry is preserved, the off-shell scattering T matrix for the dynamic problem under consideration becomes a supermatrix that connects the expansion coefficients of beams with different frequencies ω_n , but each submatrix (n, n') remains diagonal and independent of m , i.e.,

$$a_{p\ell m}^{+(n)} = \sum_{n'} T_{p\ell}^{nn'} a_{p\ell m}^{0(n')}. \quad (2)$$

For a monochromatic incident wave of angular frequency ω , the scattered field consists of an infinite number of beams with angular frequencies ω_n emerging from elastic ($n = 0$) and inelastic ($n \neq 0$) scattering. In practice, we truncate all infinite series involved at a maximum order $|n| = N$. The resulting normalized (dimensionless) scattering cross section, averaged

over a period of the radius variation, is given by [37]

$$\sigma_{\text{sc}} = \sum_{n=-N}^N \frac{2}{(k_n R_0)^2} \sum_{\ell} (2\ell + 1) |T_{\ell}^{n0}|^2, \quad (3)$$

where $k_n = \omega_n \sqrt{\epsilon \mu} / c$. We note that here, in the fully dynamic description of the problem, EM energy is not conserved even in the absence of material losses and can be exchanged with the sphere vibration. In this respect, absorption or gain can occur even with particles made of completely lossless and passive materials. The corresponding absorption cross section takes the form [37]

$$\sigma_{\text{abs}} = - \sum_{n=-N}^N \frac{2}{(k_n R_0)^2} \sum_{\ell} (2\ell + 1) \{ |T_{\ell}^{n0}|^2 + \text{Re}[T_{\ell}^{n0}] \delta_{n0} \}. \quad (4)$$

This approach is general and applies to any type of periodic variation of the sphere radius. In this respect, damped vibrations or pulses can also be studied by considering periodically repeating pulse trains. However, in these cases, an increased truncation order N is usually required to describe accurately the vibration of the sphere.

B. The adiabatic quasistatic approximation

Since we are mainly interested in periodic oscillations of the radius which are very slow compared to the variation of the EM field, it is worth comparing our fully dynamic solution with the adiabatic quasistatic approximation. In this approximation, the dynamic process is described as a sequence of snapshots of the vibration evolution, and we can introduce time-dependent coefficients $a_{\ell m}^+(t)$ for the scattered field that result from a time-dependent scattering T matrix, assuming they are constant over a period of the EM wave. The quasistatic (QS) normalized scattering cross section is calculated as

$$\sigma_{\text{sc};\text{QS}}(t) = \frac{1}{(k_0 R_0)^2 |\mathbf{E}_0|^2} \sum_{\ell m} |a_{\ell m}^+(t)|^2. \quad (5)$$

Since the scattered field is periodic with angular frequency Ω , the scattering cross section can be expanded in a Fourier series as detailed in Ref. [41]:

$$\sigma_{\text{sc};\text{QS}}(t) = \sum_{n=0, \pm 1, \dots} \sigma_{\text{sc};\text{QS}}^{(n)} e^{in\Omega t}. \quad (6)$$

It is worth noting that this approach is valid only in the limit $\Omega/\omega \rightarrow 0$, as shown in Ref. [37] and discussed also in the next section.

III. RESULTS AND DISCUSSION

We shall study the optical response of a homogeneous spherical particle of radius R_0 , dielectric permittivity $\epsilon_M = 12$, and magnetic permeability $\mu_M = 1$, which is appropriate for silicon, subject to a sinusoidal variation of the radius with angular frequency Ω . The particle is embedded in air and illuminated by a plane EM wave of angular frequency ω . We focus on the first-order TE Mie mode of the particle with angular momentum $\ell = 12$ (TE $_{\ell=12}$) at $\omega_r = 4.6422c/R_0$. This resonance has a rather high quality factor $Q = \omega_r/2\gamma \approx$

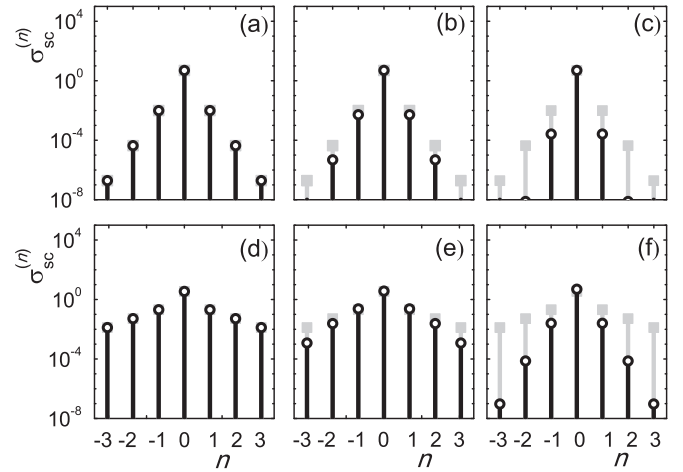


FIG. 2. Fourier components of the optical scattering cross section for a silicon sphere with a time-varying radius, $R(t) = R_0[1 + \eta \cos(\Omega t)]$, for incident light of angular frequency $\omega = \omega_r$ (see Fig. 1). Results obtained with the fully dynamic time Floquet method (black symbols) and with the adiabatic quasistatic approximation (gray symbols) for (a) $\Omega = \gamma/6$, $\eta = 10^{-10}$, (b) $\Omega = \gamma$, $\eta = 10^{-10}$, (c) $\Omega = 6\gamma$, $\eta = 10^{-10}$, (d) $\Omega = \gamma/6$, $\eta = 10^{-9}$, (e) $\Omega = \gamma$, $\eta = 10^{-9}$, and (f) $\Omega = 6\gamma$, $\eta = 10^{-9}$.

6.8×10^8 , where γ is its half-width at half maximum, and the corresponding electric field profile is shown in Fig. 1(a). The scattering cross section in the vicinity of the resonance for the static particle is presented in Fig. 1(b) by the solid black line. When the particle vibrates with an angular frequency Ω we expect scattering at frequencies ω_n around the frequency of the incoming light, as is schematically depicted in Fig. 1(a).

In the quasistatic picture, subsequent snapshots of the vibration are considered, and the optical spectrum exhibits a rigid shift following the variation of the radius [33]. In the case of our homogeneous and dispersionless dielectric scatterer, due to the scaling properties of Maxwell equations, changes in the radius $R(t) = R_0[1 + \eta \cos(\Omega t)]$ result in a temporal variation of the optical resonance frequency

$$\omega_r(t) = \omega_r \frac{1}{1 + \eta \cos(\Omega t)} \approx \omega_r [1 - \eta \cos(\Omega t)], \quad \eta \ll 1, \quad (7)$$

where η is the relative oscillation amplitude of the radius. In Fig. 1(b) we see the maximum shift of the optical scattering cross section spectrum of a static particle of radius $R_0(1 - \eta)$ for $\eta = 10^{-10}$ and $\eta = 10^{-9}$. In the latter case, the maximum shift of the resonance exceeds its half-width at half maximum γ , so we expect abrupt changes in the scattering cross section within one vibration period.

We next consider a dynamic sphere with its radius vibrating sinusoidally and present results for different vibration frequencies and amplitudes. In Fig. 2 we compare the Fourier components of the scattering cross section obtained using the time-Floquet method and the quasistatic approximation. The incident light frequency is fixed on resonance ($\omega = \omega_r$). The top panels show the results for the smaller vibration amplitude, $\eta = 10^{-10}$, and vibration frequencies $\Omega = \gamma/6$ [Fig. 2(a)], $\Omega = \gamma$ [Fig. 2(b)], and $\Omega = 6\gamma$ [Fig. 2(c)]. In this

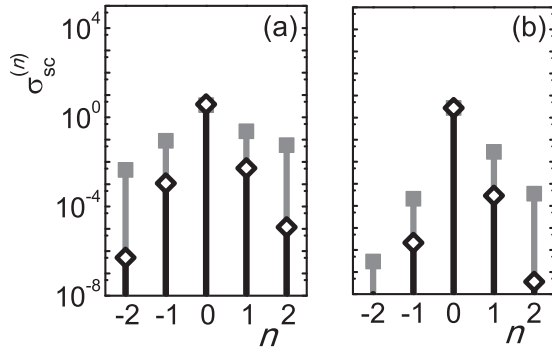


FIG. 3. Fourier components of the optical scattering cross section for a silicon sphere with a time-varying radius $R(t) = R_0[1 + \eta \cos(\Omega t)]$ (see Fig. 1). (a) Results for incoming light frequency $\omega = \omega_r + \gamma$ and vibration frequency $\Omega = \gamma$. (b) Results for incoming light frequency $\omega = \omega_r + 6\gamma$ and vibration frequency $\Omega = 6\gamma$. Open symbols correspond to $\eta = 10^{-10}$, and solid squares correspond to $\eta = 10^{-9}$.

case we see that the quasistatic approximation (gray bars and symbols) generally overestimates the higher-order inelastic scattering components and this discrepancy is more pronounced in the case of the higher vibration frequency $\Omega = 6\gamma$. For lower values of Ω the differences between the quasistatic and the fully dynamic calculations are smaller [37]. For the larger vibration amplitude, $\eta = 10^{-9}$, the interaction between light and sphere vibration is stronger, which is manifested in a slower decay of the inelastic scattering intensities, as shown in Figs. 2(d) to 2(f). Probing the particle on resonance results in symmetric Stokes and anti-Stokes components, as expected for a symmetric resonance line shape with respect to ω_r . Generally, the adiabatic quasistatic approximation works reasonably well for low vibration frequencies but overestimates the inelastic scattering intensities as the vibration frequency increases.

We proceed by considering the scattering of light at frequencies detuned from the optical resonance at ω_r . In particular, in order to observe resonant phenomena, we discuss two cases: first, for a vibration frequency $\Omega = \gamma$ and light frequency $\omega = \omega_r + \gamma$ and, second, for $\Omega = 6\gamma$ and $\omega = \omega_r + 6\gamma$. The corresponding Fourier components of the scattering cross section, calculated using the time-Floquet method, are shown in Figs. 3(a) and 3(b), respectively, for the two vibration amplitudes, $\eta = 10^{-10}$ and $\eta = 10^{-9}$. In typical BLS experiments [42–44], the regime of $\Omega \lesssim \gamma$ depicted in Fig. 3(a) is often termed the *nonresolved-sideband* regime [45–47], while the regime when $\Omega > \gamma$ presented in Fig. 3(b) is called the *resolved-sideband* regime [48–50]. Generally, the strength of the inelastic components shows trends similar to the case of zero detuning ($\omega = \omega_r$) discussed above. However, detuning results in an asymmetry of the Stokes and anti-Stokes scattering intensities, as shown in Figs. 3(a) and 3(b). Interestingly, in the resolved-sideband case [Fig. 3(b)], the asymmetry is stronger, while for incident light with $\omega = \omega_r - \Omega$, the ratio between the $n = 1$ and $n = -1$ components is inverted, which is a direct consequence of the symmetry of the optical resonance around ω_r .

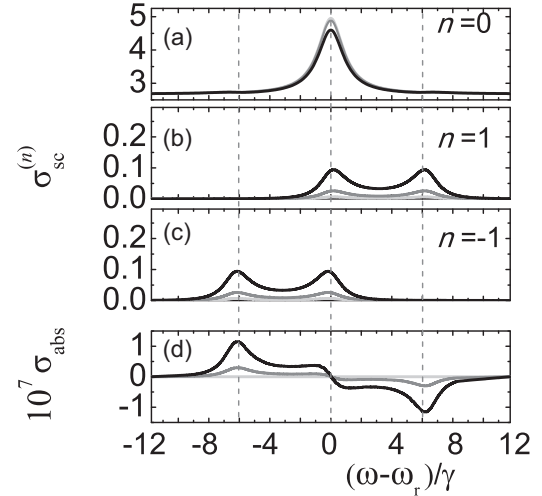


FIG. 4. From top to bottom: Fourier components of the optical scattering cross section $\sigma_{sc}^{(n)}$ for $n = 0, \pm 1$ and absorption cross section σ_{abs} of a silicon sphere with radius $R(t) = R_0[1 + \eta \cos(\Omega t)]$ vibrating with frequency $\Omega = 6\gamma$ versus the frequency detuning $\omega - \omega_r$ of the incoming light from the first-order $\text{TE}_{\ell=12}$ Mie resonance for three different vibration amplitudes: $\eta = 5 \times 10^{-10}$ (light gray line), $\eta = 10^{-9}$ (dark gray line), and $\eta = 2 \times 10^{-9}$ (black line).

Next, we fix the vibration frequency of the radius and scan over the frequency of the incoming light. In Figs. 4(a), 4(b) and 4(c) we present the variation of the elastic ($n = 0$) and inelastic ($n = \pm 1$) scattering intensities under a sinusoidal vibration of the sphere radius with frequency $\Omega = 6\gamma$. Each one of the three curves in each diagram corresponds to different values of the vibration amplitude, namely, $\eta = 5 \times 10^{-10}$, $\eta = 10^{-9}$, and $\eta = 2 \times 10^{-9}$. When $\Omega = 6\gamma$ we are in the weak-coupling, resolved-sideband regime. As we increase the amplitude of the oscillation, we see increased scattering in the first-order inelastic beams ($n = \pm 1$), manifested as a double-peak structure with maxima at ω_r and $\omega_r \mp \Omega$, respectively, which correspond to high initial and final optical densities of states in the respective photon transitions. Apart from a redistribution of light intensity to different frequencies, the vibration leads to absorption or gain of energy, which is manifested in the absorption cross section [see Eq. (4)] displayed in Fig. 4(d). As already discussed previously [37], contrary to the adiabatic approximation, the fully dynamic description is able to account for the exchange of energy between the optical and vibrational modes. Again, due to the symmetry of the optical resonance, the absorption curves are antisymmetric with respect to ω_r . Another interesting point is that the energy transfer increases with the oscillation amplitude.

When the frequency of the vibration is of the order of the half-width of the optical resonance γ , the behavior of the system shows some remarkable features. This is depicted in Fig. 5, where we present the results for the elastic and inelastic components of the scattering cross section for $\Omega = \gamma$. For small vibration amplitudes ($\eta = 5 \times 10^{-10}$, light gray curves), the calculations show an elastic scattering peak at $\omega = \omega_r$, but the $n = 1$ ($n = -1$) inelastic scattering intensities exhibit a maximum at frequencies which are smaller than $-\Omega$ (Ω). This is different from the behavior discussed previously for the

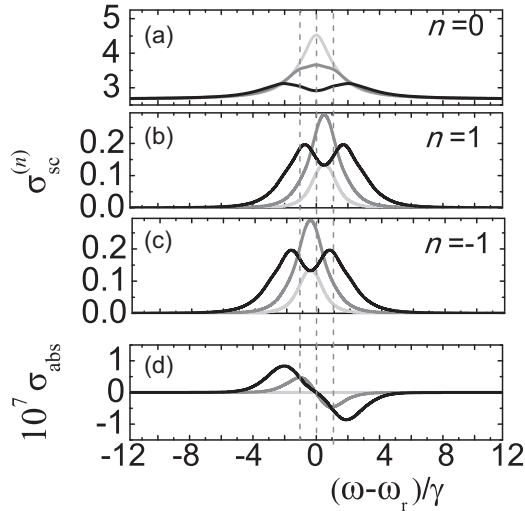


FIG. 5. From top to bottom: Fourier components of the optical scattering cross section $\sigma_{sc}^{(n)}$ for $n = 0, \pm 1$ and absorption cross section σ_{abs} of a silicon sphere with radius $R(t) = R_0[1 + \eta \cos(\Omega t)]$ vibrating with frequency $\Omega = \gamma$ versus the frequency detuning $\omega - \omega_r$ of the incoming light from the first-order $TE_{\ell=12}$ Mie resonance for three different vibration amplitudes: $\eta = 5 \times 10^{-10}$ (light gray line), $\eta = 10^{-9}$ (dark gray line), and $\eta = 2 \times 10^{-9}$ (black line).

weak-coupling regime. By increasing the vibration amplitude ($\eta = 10^{-9}$, dark gray curves), we observe a decrease in the elastic scattering intensity followed by a respective increase in the inelastically scattered beams. For higher vibration amplitudes ($\eta = 2 \times 10^{-9}$, black curves), we see a splitting in both the elastic and inelastic scattering components. The occurrence of this splitting indicates strong coupling in systems of coupled oscillators [51,52] and has also been observed in optomechanical systems as well as in the coupling of EM radiation with atoms and molecules (Rabi splitting). However, in our case here, this is due to the parametric coupling of the mechanical vibration with the optical resonator, which have very dissimilar frequencies.

The mode splitting mentioned here can be explained by invoking a mechanical analog, namely, a driven oscillator with displacement x and periodically varying eigenfrequency $\omega_r(t)$, given by Eq. (7). For $\eta \ll 1$, we have $\omega_r^2(t) \approx \omega_r^2[1 - 2\eta \cos(\Omega t)]$, and in the absence of external stimulus, we can look for the normal modes solving the homogeneous differential equation

$$\frac{d^2x(t)}{dt^2} + \omega_r^2[1 - 2\eta \cos(\Omega t)]x(t) = 0. \quad (8)$$

Equation (8) is the so-called Mathieu's equation [53], introduced more than a century ago for the description of a variety of forced mechanical oscillators. In the special case considered here and in the quasistatic adiabatic limit ($\Omega/\omega \rightarrow 0$), we can find analytical solutions of Eq. (8) (see Appendix B). The normal modes with maximum projection on the elastic scattering component ($n = 0$) are those with the largest detuning from ω_r . If ω_+ and ω_- are the corresponding eigenfrequencies, we obtain a mode splitting that varies linearly with η ,

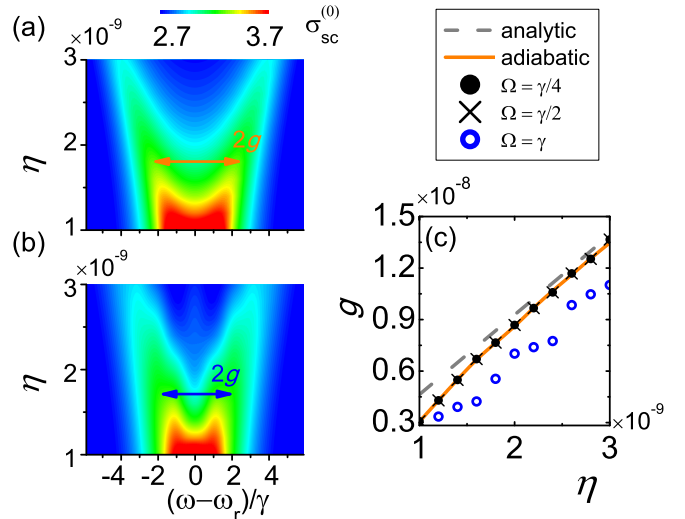


FIG. 6. (a) Elastic Fourier component ($n = 0$) of the optical scattering cross section of a silicon sphere with an oscillating radius, $R(t) = R_0[1 + \eta \cos(\Omega t)]$, calculated by the adiabatic quasistatic approximation ($\Omega/\omega \rightarrow 0$) versus the vibration amplitude η and the frequency detuning $\omega - \omega_r$ of the incoming light from the first-order $TE_{\ell=12}$ Mie resonance. (b) The same as in (a) for $\Omega = \gamma$ (fully dynamic calculations). (c) Variation of the parametric-coupling constant g obtained from the frequency difference between the two peaks of the elastic scattering cross-section component, with the vibration amplitude, for different vibration frequencies Ω . Solid circles, crosses, and open circles correspond to fully dynamic calculations for $\Omega = \gamma/4$, $\Omega = \gamma/2$, and $\Omega = \gamma$ [taken from (b)], respectively. The dashed gray line corresponds to Eq. (9), and the orange solid line is obtained from the adiabatic spectra shown in (a).

following Eq. (B5):

$$\omega_+ - \omega_- \equiv 2g \simeq 2\eta\omega_r, \quad (9)$$

where g defines the parametric-coupling constant. On the other hand, numerical calculations can easily be carried out in the framework of the adiabatic quasistatic approximation, as described in Sec. II B. In Fig. 6(a) we show the elastic scattering cross-section spectra $\sigma_{sc}^{(0)}$ for different vibration amplitudes η , calculated using the adiabatic quasistatic approximation, and mark the characteristic splitting $2g$ that increases with increasing η . The values of g obtained in this manner are depicted in Fig. 6(c) by the orange solid line, while the analytic expression of Eq. (9) is presented by the dashed gray line. The two lines are in rough agreement, indicating that the mechanical analog can provide an approximate description of the behavior of the actual system. For comparison, we also show the results of fully dynamic calculations using our time-Floquet method for very small values of Ω , namely, $\Omega = \gamma/4$ and $\Omega = \gamma/2$. The coincidence is obvious.

Let us now examine what happens when Ω increases and the system deviates from the adiabatic limit. In particular, we set $\Omega = \gamma$, which is the case studied in Fig. 5. In Fig. 6(b) we show $\sigma_{sc}^{(0)}$ for different values of η . Figure 6(b) is a more detailed version of Fig. 5(a). The spectra of $\sigma_{sc}^{(0)}$ for relatively small values of η begin with a single peak, which then splits into two distinct modes for $\eta = 1.2 \times 10^{-9}$ to $\eta = 1.4 \times 10^{-9}$. This splitting, marked as $2g$, is also plotted in Fig. 6(c) with

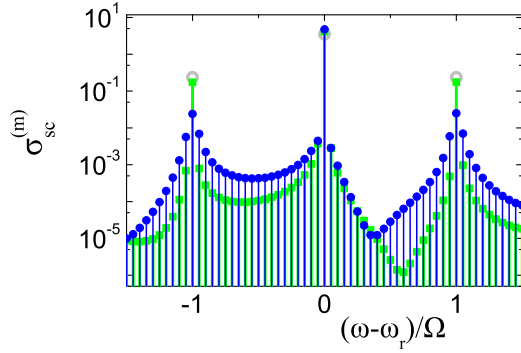


FIG. 7. Fourier components of the optical scattering cross section of a silicon sphere with a radius oscillating according to Eq. (10), with angular frequency $\Omega = \gamma$, amplitude $\eta = 10^{-9}$, and two different damping constants: $\Gamma = 0.033\gamma$ (green squares) and $\Gamma = 0.2\gamma$ (blue circles). The incoming light impinges on resonance $\omega = \omega_r$ (see Fig. 1). The damped oscillations have a repetition period $\tau = 20T$, which produces the fine-grained Fourier spectrum. The gray open symbols show the Fourier components for the undamped vibration, depicted also in Fig. 2(c).

open symbols. However, now, for higher values of η the spectrum is more complex, and more side peaks appear. In this regime, for higher Ω , the simple analytic approximation for the parametric-coupling constant g is no longer valid, and fully dynamical computations are required.

In actual implementations, damping of optical and mechanical oscillators cannot be avoided and could significantly influence effects which are based on high-quality-factor resonators, such as those we consider in the present study. Optical losses are expected to broaden the Mie resonances. These losses can easily be included in our study, and their influence can readily be estimated. However, the influence of damping in the elastic vibration is worth a closer investigation. Our time-Floquet method is valid for periodic variations of the radius, so a damped vibration can be simulated as a periodic sequence of decaying vibrations with a sufficiently long repetition period $\tau \gg T$. We consider such a pulse train of damped vibrations with frequency Ω and damping rate Γ ,

$$R(t) = \sum_{p=-\infty}^{\infty} \Pi(t - p\tau) R_0 [1 + \eta e^{-\Gamma(t-p\tau)} \cos[\Omega(t - p\tau)]], \quad (10)$$

where $\Pi(t) = 1$ for $0 < t < \tau$ and 0 otherwise. The long period τ is independent of the vibration frequency Ω and controls only the discretization in the frequency domain. In Fig. 7 we show the Fourier components of the optical scattering cross section of the vibrating sphere under consideration for a relatively small damping constant, $\Gamma = 0.033\gamma$. As Γ increases, the amplitude of the Fourier components ($n = \pm 1$, in Fig. 2) decreases while contributions from frequencies around Ω grow in magnitude. In particular, the elastic Fourier component $\sigma_{sc}^{(0)}$ increases by approximately 12% for $\Gamma = 0.033\gamma$ and 30% for $\Gamma = 0.2\gamma$ compared to the case without dumping ($\Gamma = 0$, gray symbols), while the inelastic scattering intensities at $\omega - \omega_r = \pm\Omega$ are reduced by 26% for $\Gamma = 0.033\gamma$ and by almost 90% for $\Gamma = 0.2\gamma$.

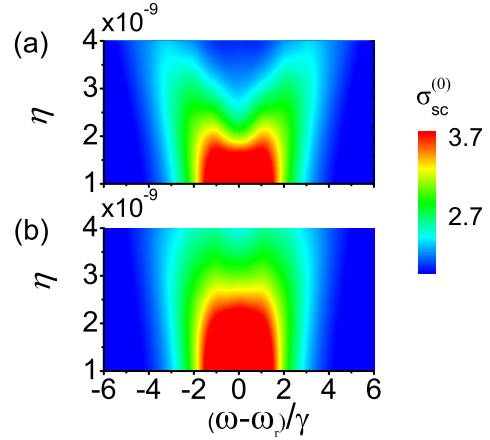


FIG. 8. Elastic Fourier component ($n = 0$) of the optical scattering cross section of a silicon sphere undergoing damped vibrations with angular frequency $\Omega = \gamma$ and decay rate: (a) $\Gamma = 0.033\gamma$ and (b) $\Gamma = 0.066\gamma$ versus the vibration amplitude η and the frequency detuning $\omega - \omega_r$ of the incoming light from the first-order $\text{TE}_{\ell=12}$ Mie resonance.

We now examine the impact of mechanical damping on the results displayed in Fig. 6(b). In Fig. 8(a) we show the corresponding $\sigma_{sc}^{(0)}$ spectra for the same vibration frequency $\Omega = \gamma$ with a decay rate $\Gamma = 0.033\gamma$ for amplitudes ranging from $\eta = 10^{-9}$ to $\eta = 4 \times 10^{-9}$. It can be seen that vibration damping hinders the appearance of parametric mode splitting, which is the fingerprint of the strong-coupling regime, and this splitting occurs at higher vibration amplitudes η , while all other spectral features are slightly smoothed and reduced. This is more clearly manifested if we increase the decay constant, as shown in Fig. 8(b) for $\Gamma = 0.066\gamma$. Quite generally, mode splitting in the strong-coupling regime is washed out by mechanical damping; however, it can still be recovered for larger vibration amplitudes. Optical absorption also has a similar effect. For example, assuming an imaginary part in the permittivity $\text{Im}\{\epsilon\} = 10^{-4}$, the vibration amplitude η required to achieve the mode-splitting characteristic of the strong-coupling regime increases by almost two orders of magnitude. Frequency dispersion can also be taken into account, e.g., along the lines suggested in Refs. [54,55].

The effects discussed above can also be reproduced with other modes with different ℓ ; however, there are differences. Generally, lower- ℓ modes have lower quality factors. This means that they are less sensitive, and thus, larger vibration amplitudes η are required to achieve similar effects. On the other hand, sensitivity increases for modes that confine the EM field closer to the surface of the particle, which results in better coupling with the breathing mode. The $\ell = 12$ mode, discussed here, was chosen as an example of a high-quality-factor resonant mode with a field profile confined close to the particle surface [see Fig. 1(a)]. Apart from the dependence of the optical-vibrational coupling constant g on the optical mode profile, we found no distinctive difference between TE and TM modes. The influence of a periodically varying radius on a resonant optical mode of a dielectric sphere should be observable at different length scales. The vibration frequency required is controlled by the quality factor of the optical

resonance. For light in the visible and infrared, the vibration frequency can vary from megahertz to gigahertz for micron-sized particles, which is experimentally achievable [21,56,57]. As an indicative example, for a particle of radius $R_0 = 1 \mu\text{m}$, the optical resonance frequency is $\omega_r \simeq 2\pi \times 222 \text{ THz}$, and the corresponding half-width at half maximum $\gamma \simeq 1 \text{ MHz}$, indicating vibrational frequencies on the order of megahertz.

IV. CONCLUSIONS

In summary, we presented an extension of Mie theory to the case of a spherical scatterer with a periodically time varying radius using a time-Floquet method. Elastic and inelastic cross-section spectra, in the vicinity of a high- Q Mie resonance, were analyzed in conjunction with the quasistatic adiabatic approximation, providing a consistent interpretation of the underlying physics. In the weak-coupling regime, perturbation theory predicts enhanced inelastic scattering to frequencies of high optical densities of states. Therefore, if the incident wave is red- or blueshifted from the resonance frequency, stronger anti-Stokes or Stokes intensities are favored, leading to resonant energy transfer from the oscillating sphere to the EM field (optical gain) or vice versa (optical losses). This effect, which cannot be accounted for by the adiabatic approach, becomes more pronounced as the oscillation amplitude increases and higher-order inelastic components become progressively important. In the strong-coupling regime, we reveal the occurrence of parametric interaction effects which, with an increase in the vibration amplitude, lead to a splitting in both elastic and inelastic scattering components, as predicted by the solutions of Mathieu's equation in the proper limit. Finally, vibration damping results in reduced inelastic scattering effects and hinders parametric mode splitting.

ACKNOWLEDGMENTS

The authors acknowledge fruitful discussions with Dr. P. A. Pantazopoulos and I. Stefanou. E.P. acknowledges support for this research, which is cofinanced by Greece and the European Union [European Social Fund (ESF)] through the Operational Programme "Human Resources Development, Education and Lifelong Learning" in the context of the project "Strengthening Human Resources Research Potential via Doctorate Research" (MIS-5000432), implemented by the State Scholarships Foundation (IKY).

APPENDIX A: SCATTERING T MATRIX FOR A SPHERE WITH A PERIODICALLY TIME VARYING RADIUS

Electromagnetic scattering by a homogeneous sphere with a periodically time varying radius, $R(t) = R(t + T)$, can be efficiently described by the T -matrix method. We assume that the sphere has a relative permittivity ϵ_M and permeability μ_M and is embedded in a homogeneous medium characterized by relative permittivity and permeability ϵ and μ , respectively. There have been several works dealing with wave scattering from dynamically varying objects, among which are a formal generalization of multiple-scattering theory to time-varying elastic scatterers [58] and a theoretical treatment

of a spatiotemporally modulated ultrasonic circulator [59]. More recently, light scattering by a sphere with a periodically varying refractive index was also elaborated [37,54,55]. Here, we restrict our analysis to periodic oscillations of the sphere radius. The effect of decaying oscillation amplitudes can also be considered by assuming a periodic train of decaying pulses [58].

In a periodically varying medium, the electric component of the EM field can be written in the Floquet form

$$\mathbf{E}(\mathbf{r}, t) = \sum_{n=-\infty}^{\infty} \text{Re}[\mathbf{E}^{(n)}(\mathbf{r}) \exp(-i\omega_n t)], \quad (\text{A1})$$

with a similar expression for the magnetic component $\mathbf{H}(\mathbf{r}, t)$. The period T of the vibration determines the frequencies of the different beams $\omega_n = \omega - n\Omega$, where ω is the Floquet quasifrequency, $\Omega = 2\pi/T$, and $n = 0, \pm 1, \pm 2, \dots$. The electric and magnetic components of an incoming EM field ($\mathbf{E}_0, \mathbf{H}_0$) are expanded in a spherical-wave basis,

$$\mathbf{E}_0^{(n)}(\mathbf{r}) = \sum_{\ell=1}^{\infty} \sum_{m=-\ell}^{\ell} \left[\frac{i}{k_n} a_{E\ell m}^{0(n)} \nabla \times j_{\ell}(k_n r) \mathbf{X}_{\ell m}(\hat{\mathbf{r}}) + a_{H\ell m}^{0(n)} j_{\ell}(k_n r) \mathbf{X}_{\ell m}(\hat{\mathbf{r}}) \right], \quad (\text{A2})$$

$$\mathbf{H}_0^{(n)}(\mathbf{r}) = \sqrt{\frac{\epsilon\epsilon_0}{\mu\mu_0}} \sum_{\ell=1}^{\infty} \sum_{m=-\ell}^{\ell} \left[a_{E\ell m}^{0(n)} j_{\ell}(k_n r) \mathbf{X}_{\ell m}(\hat{\mathbf{r}}) - \frac{i}{k_n} a_{H\ell m}^{0(n)} \nabla \times j_{\ell}(k_n r) \mathbf{X}_{\ell m}(\hat{\mathbf{r}}) \right], \quad (\text{A3})$$

where $k_n = \omega_n \sqrt{\epsilon\mu}/c$ is the corresponding wave number. The scattered field ($\mathbf{E}_{\text{sc}}, \mathbf{H}_{\text{sc}}$) is expressed in the same manner as in Eq. (A1), while its spherical-wave expansion is similar to Eqs. (A2) and (A3) with expansion coefficients $a_{P\ell m}^{+(n)}$, $P = E, H$, instead of $a_{P\ell m}^{0(n)}$, and spherical Hankel functions h_{ℓ}^+ , which are appropriate for outgoing waves, in place of the spherical Bessel functions j_{ℓ} . Finally, the field inside the particle ($\mathbf{E}_M, \mathbf{H}_M$) is also expressed in the form of Eqs. (A1), (A2), (A3), with expansion coefficients $a_{P\ell m}^{M(n)}$ and wave number $q_n = \omega_n \sqrt{\epsilon_M \mu_M}/c$ instead of k_n in the argument of the spherical Bessel functions.

Continuity of the tangential components of the (complex) EM field at the vibrating surface of the sphere for every time t is expressed through the equations

$$\mathbf{X}_{\ell m}^*(\hat{\mathbf{r}}) \cdot (\mathbf{E}_0 + \mathbf{E}_{\text{sc}} - \mathbf{E}_M) = 0, \quad (\text{A4})$$

$$[\hat{\mathbf{r}} \times \mathbf{X}_{\ell m}^*(\hat{\mathbf{r}})] \cdot (\mathbf{E}_0 + \mathbf{E}_{\text{sc}} - \mathbf{E}_M) = 0, \quad (\text{A5})$$

$$\mathbf{X}_{\ell m}^*(\hat{\mathbf{r}}) \cdot (\mathbf{H}_0 + \mathbf{H}_{\text{sc}} - \mathbf{H}_M) = 0, \quad (\text{A6})$$

$$[\hat{\mathbf{r}} \times \mathbf{X}_{\ell m}^*(\hat{\mathbf{r}})] \cdot (\mathbf{H}_0 + \mathbf{H}_{\text{sc}} - \mathbf{H}_M) = 0. \quad (\text{A7})$$

One can proceed further by taking advantage of the following properties of the vector spherical harmonics:

$$\int \mathbf{X}_{\ell m}^*(\hat{\mathbf{r}}) \cdot \mathbf{X}_{\ell' m'}(\hat{\mathbf{r}}) d\hat{\mathbf{r}} = \delta_{\ell\ell'} \delta_{mm'}, \quad (\text{A8})$$

$$\int [\hat{\mathbf{r}} \times \mathbf{X}_{\ell m}^*(\hat{\mathbf{r}})] \cdot \mathbf{X}_{\ell' m'}(\hat{\mathbf{r}}) d\hat{\mathbf{r}} = 0, \quad (\text{A9})$$

$$\int \mathbf{X}_{\ell m}^*(\hat{\mathbf{r}}) \cdot [\nabla \times f_{\ell'}(kr) \mathbf{X}_{\ell' m'}(\hat{\mathbf{r}})] d\hat{\mathbf{r}} = 0, \quad (\text{A10})$$

$$\begin{aligned} & \int [\hat{\mathbf{r}} \times \mathbf{X}_{\ell m}^*(\hat{\mathbf{r}})] \cdot [\nabla \times f_{\ell'}(kr) \mathbf{X}_{\ell' m'}(\hat{\mathbf{r}})] d\hat{\mathbf{r}} \\ &= \frac{1}{r} \frac{\partial}{\partial r} [r f_{\ell'}(kr)] \delta_{\ell \ell'} \delta_{m m'}, \end{aligned} \quad (\text{A11})$$

where f_{ℓ} can be any linear combination of the spherical Bessel and Hankel functions.

Integrating Eq. (A4) over the surface of a sphere with radius $R(t)$, with the help of the above properties, one obtains

$$\begin{aligned} & \sum_{n=-\infty}^{\infty} [a_{H\ell m}^{0(n)} j_{\ell}(k_n R(t)) + a_{H\ell m}^{+(n)} h_{\ell}^+(k_n R(t)) \\ & - a_{H\ell m}^{M(n)} j_{\ell}(q_n R(t))] \exp(-i\omega_n t) = 0. \end{aligned} \quad (\text{A12})$$

Similar expressions result from the other boundary condition equations. We now expand the spherical Bessel and Hankel functions of time-dependent argument into Fourier series,

$$j_{\ell}(k_n R(t)) = \sum_{p=-\infty}^{\infty} A_{p,n}^{(\ell)} \exp(ip\Omega t), \quad (\text{A13})$$

$$h_{\ell}^+(k_n R(t)) = \sum_{p=-\infty}^{\infty} B_{p,n}^{(\ell)} \exp(ip\Omega t), \quad (\text{A14})$$

$$j_{\ell}(q_n R(t)) = \sum_{p=-\infty}^{\infty} C_{p,n}^{(\ell)} \exp(ip\Omega t), \quad (\text{A15})$$

$$\frac{1}{x} [x j_{\ell}(x)]' \Big|_{x=q_n R(t)} = \sum_{p=-\infty}^{\infty} D_{p,n}^{(\ell)} \exp(ip\Omega t), \quad (\text{A16})$$

$$\frac{1}{x} [x h_{\ell}^+(x)]' \Big|_{x=k_n R(t)} = \sum_{p=-\infty}^{\infty} E_{p,n}^{(\ell)} \exp(ip\Omega t), \quad (\text{A17})$$

$$\frac{1}{x} [x j_{\ell}(x)]' \Big|_{x=k_n R(t)} = \sum_{p=-\infty}^{\infty} F_{p,n}^{(\ell)} \exp(ip\Omega t), \quad (\text{A18})$$

and introducing $n' = n + p$, we obtain the following set of four linear equations for every n', l, m :

$$\sum_{n=-\infty}^{\infty} \left(-B_{n'-n,n}^{(\ell)} a_{H\ell m}^{+(n)} + C_{n'-n,n}^{(\ell)} a_{H\ell m}^{M(n)} \right) = \sum_{n=-\infty}^{\infty} A_{n'-n,n}^{(\ell)} a_{H\ell m}^{0(n)}, \quad (\text{A19})$$

$$\begin{aligned} & \sum_{n=-\infty}^{\infty} \left(-E_{n'-n,n}^{(\ell)} a_{H\ell m}^{+(n)} + \sqrt{\frac{\epsilon_M \mu}{\epsilon_M \mu}} D_{n'-n,n}^{(\ell)} a_{H\ell m}^{M(n)} \right) \\ &= \sum_{n=-\infty}^{\infty} F_{n'-n,n}^{(\ell)} a_{H\ell m}^{0(n)}, \end{aligned} \quad (\text{A20})$$

$$\begin{aligned} & \sum_{n=-\infty}^{\infty} \left(-B_{n'-n,n}^{(\ell)} a_{E\ell m}^{+(n)} + \sqrt{\frac{\epsilon_M \mu}{\epsilon_M \mu}} C_{n'-n,n}^{(\ell)} a_{E\ell m}^{M(n)} \right) \\ &= \sum_{n=-\infty}^{\infty} A_{n'-n,n}^{(\ell)} a_{E\ell m}^{0(n)}, \end{aligned} \quad (\text{A21})$$

$$\begin{aligned} & \sum_{n=-\infty}^{\infty} \left(-E_{n'-n,n}^{(\ell)} a_{E\ell m}^{+(n)} + D_{n'-n,n}^{(\ell)} a_{E\ell m}^{M(n)} \right) \\ &= \sum_{n=-\infty}^{\infty} F_{n'-n,n}^{(\ell)} a_{E\ell m}^{0(n)}. \end{aligned} \quad (\text{A22})$$

It is worth noting that, since the spherical symmetry of the vibrating particle is conserved, the polarization (E, H) and angular momentum (ℓ) modes are decoupled, while m is immaterial; that is, the solution of Eqs. (A19) to (A22) does not depend on the value of m . In practice, the above infinite system of equations is truncated to a maximum order $n = N$. By defining the block matrices $\mathbf{M}^{(\ell)}$, with elements $M_{n'-n,n}^{(\ell)}$, for $M = A, B, C, D, E, F$, with dimensions $(2N+1) \times (2N+1)$, the system of equations can be cast in matrix form,

$$\begin{pmatrix} -\mathbf{B}^{(\ell)} & \mathbf{C}^{(\ell)} \\ -\mathbf{E}^{(\ell)} & \sqrt{\frac{\epsilon_M \mu}{\epsilon_M \mu}} \mathbf{D}^{(\ell)} \end{pmatrix} \begin{pmatrix} \mathbf{a}_{H\ell m}^+ \\ \mathbf{a}_{H\ell m}^M \end{pmatrix} = \begin{pmatrix} \mathbf{A}^{(\ell)} \mathbf{a}_{H\ell m}^0 \\ \mathbf{F}^{(\ell)} \mathbf{a}_{H\ell m}^0 \end{pmatrix}, \quad (\text{A23})$$

$$\begin{pmatrix} -\mathbf{B}^{(\ell)} & \sqrt{\frac{\epsilon_M \mu}{\epsilon_M \mu}} \mathbf{C}^{(\ell)} \\ -\mathbf{E}^{(\ell)} & \mathbf{D}^{(\ell)} \end{pmatrix} \begin{pmatrix} \mathbf{a}_{E\ell m}^+ \\ \mathbf{a}_{E\ell m}^M \end{pmatrix} = \begin{pmatrix} \mathbf{A}^{(\ell)} \mathbf{a}_{E\ell m}^0 \\ \mathbf{F}^{(\ell)} \mathbf{a}_{E\ell m}^0 \end{pmatrix}, \quad (\text{A24})$$

where $\mathbf{a}_{p\ell m}^{0,+M} \equiv [a_{p\ell m}^{0,+M(-N)}, a_{p\ell m}^{0,+M(-N+1)}, \dots, a_{p\ell m}^{0,+M(N)}]^T$ are column vectors of dimension $2N+1$.

Solving for the coefficients of the scattered field, we have

$$\begin{aligned} \mathbf{a}_{H\ell m}^+ &= \left[\mathbf{B}^{(\ell)} - \sqrt{\frac{\epsilon_M \mu}{\epsilon_M \mu}} \mathbf{C}^{(\ell)} (\mathbf{D}^{(\ell)})^{-1} \mathbf{E}^{(\ell)} \right]^{-1} \\ &\times \left[\sqrt{\frac{\epsilon_M \mu}{\epsilon_M \mu}} \mathbf{C}^{(\ell)} (\mathbf{D}^{(\ell)})^{-1} \mathbf{F}^{(\ell)} - \mathbf{A}^{(\ell)} \right] \mathbf{a}_{H\ell m}^0, \end{aligned} \quad (\text{A25})$$

$$\begin{aligned} \mathbf{a}_{E\ell m}^+ &= \left[\sqrt{\frac{\epsilon_M \mu}{\epsilon_M \mu}} \mathbf{B}^{(\ell)} - \mathbf{C}^{(\ell)} (\mathbf{D}^{(\ell)})^{-1} \mathbf{E}^{(\ell)} \right]^{-1} \\ &\times \left[\mathbf{C}^{(\ell)} (\mathbf{D}^{(\ell)})^{-1} \mathbf{F}^{(\ell)} - \sqrt{\frac{\epsilon_M \mu}{\epsilon_M \mu}} \mathbf{A}^{(\ell)} \right] \mathbf{a}_{E\ell m}^0, \end{aligned} \quad (\text{A26})$$

and the T matrix is readily deduced through Eq. (2).

APPENDIX B: MECHANICAL ANALOG TO A VIBRATING SPHERE

As discussed in the main text, the problem of the optical response of the sphere under consideration with a periodically time varying radius is equivalent to that of an oscillator with a time-varying eigenfrequency, described by Mathieu's equation [Eq. (8)]. The behavior of such a system can easily be analyzed in the special case where $\eta \ll 1$ and in the framework of the adiabatic quasistatic approximation. The normal modes are obtained by seeking Floquet solutions of the form

$$x(t) = \sum_{n=-\infty}^{\infty} A_n e^{-i(\omega-n\Omega)t}. \quad (\text{B1})$$

By truncating the sum to $2N+1$ terms, Eq. (8) leads to a system of equations expressed in matrix form as follows:

$$\begin{aligned} & \text{Band}_{2N+1} [-\omega_r^2 \eta, \omega_r^2 - (\omega - n\Omega)^2, -\omega_r^2 \eta] \\ & \times (A_{-N}, \dots, A_0, \dots, A_N)^T = 0, \end{aligned} \quad (\text{B2})$$

where by $\text{Band}_M[a, b, c]$ we denote a banded matrix of dimension $M \times M$, with a, b , and c being the elements of the lower diagonal, diagonal, and upper diagonal, respectively, and n varies from $-N$ to N along the diagonal. In the adiabatic approximation we let $\Omega \rightarrow 0$, and Eq. (B2) takes the form of the eigenvalue equation of the symmetric tridiagonal Toeplitz matrix $\text{Band}_{2N+1}[-\eta, 1, -\eta]$, which has eigenvalues [60]

$$(\omega^2/\omega_r^2)_\nu = 1 - 2\eta \cos\left(\frac{\nu\pi}{2N+2}\right) \quad (\text{B3})$$

and associated eigenvectors

$$\mathbf{A}^{(\nu)} = \left(\sin\left(\frac{\nu\pi}{2N+2}\right), \sin\left(\frac{\nu 2\pi}{2N+2}\right), \dots, \sin\left(\frac{\nu(2N+1)\pi}{2N+2}\right) \right), \quad (\text{B4})$$

where $\nu = 1, 2, \dots, 2N+1$. According to Eq. (B3), the smallest and largest eigenvalues are obtained for $\nu = 1$ and $\nu = 2N+1$, respectively, and the corresponding eigenvectors have maximum projection on the elastic component: $|A_0^{(1)}| = |A_0^{(2N+1)}| = 1$. Therefore, we expect maxima in the

elastic component at

$$\begin{aligned} \omega_- &= \omega_r \sqrt{1 - 2\eta \cos\left(\frac{\pi}{2N+2}\right)} \\ &\simeq \omega_r \left[1 - \eta \cos\left(\frac{\pi}{2N+2}\right) \right], \\ \omega_+ &= \omega_r \sqrt{1 - 2\eta \cos\left(\frac{(2N+1)\pi}{2N+2}\right)} \\ &\simeq \omega_r \left[1 - \eta \cos\left(\frac{(2N+1)\pi}{2N+2}\right) \right]. \end{aligned}$$

From the above analysis it turns out that, in the quasistatic limit ($\Omega \rightarrow 0$), the elastic ($n = 0$) component is dominated by two normal modes, separated in frequency by

$$\Delta\omega = \omega_+ - \omega_- \simeq 2\omega_r \eta \sin\left(\frac{\pi}{2}\right) \sin\left(\frac{N\pi}{2N+2}\right) \rightarrow 2\omega_r \eta. \quad (\text{B5})$$

-
- [1] N. Engheta, *Nanophotonics* **10**, 639 (2021).
[2] F. R. Morgenthaler, *IRE Trans. Microwave Theory Tech.* **6**, 167 (1958).
[3] A. Oliner and A. Hessel, *IRE Trans. Antennas Propag.* **7**, 201 (1959).
[4] J.-C. Simon, *IRE Trans. Microwave Theory Tech.* **8**, 18 (1960).
[5] D. Holberg and K. Kunz, *IEEE Trans. Antennas Propag.* **14**, 183 (1966).
[6] F. Harfoush and A. Taflove, *IEEE Trans. Antennas Propag.* **39**, 898 (1991).
[7] J. R. Zurita-Sánchez, P. Halevi, and J. C. Cervantes-Gonzalez, *Phys. Rev. A* **79**, 053821 (2009).
[8] M. C. Rechtsman, J. M. Zeuner, Y. Plotnik, Y. Lumer, D. Podolsky, F. Dreisow, S. Nolte, M. Segev, and A. Szameit, *Nature (London)* **496**, 196 (2013).
[9] E. Lustig, Y. Sharabi, and M. Segev, *Optica* **5**, 1390 (2018).
[10] N. Wang, Z.-Q. Zhang, and C. T. Chan, *Phys. Rev. B* **98**, 085142 (2018).
[11] Q. Cheng, Y. Pan, H. Wang, C. Zhang, D. Yu, A. Gover, H. Zhang, T. Li, L. Zhou, and S. Zhu, *Phys. Rev. Lett.* **122**, 173901 (2019).
[12] T. T. Koutserimpas and R. Fleury, *IEEE Trans. Antennas Propag.* **68**, 6717 (2020).
[13] B. Wang, J. Quan, J. Han, X. Shen, H. Wu, and Y. Pan, *Laser Photon. Rev.* **16**, 2100469 (2022).
[14] T. J. Kippenberg and K. J. Vahala, *Science* **321**, 1172 (2008).
[15] M. Aspelmeyer, T. J. Kippenberg, and F. Marquardt, *Rev. Mod. Phys.* **86**, 1391 (2014).
[16] Y.-L. Liu, C. Wang, J. Zhang, and Y.-X. Liu, *Chin. Phys. B* **27**, 024204 (2018).
[17] S. Viola Kusminskiy, H. X. Tang, and F. Marquardt, *Phys. Rev. A* **94**, 033821 (2016).
[18] T. Liu, X. Zhang, H. X. Tang, and M. E. Flatté, *Phys. Rev. B* **94**, 060405(R) (2016).
[19] D. Lachance-Quirion, Y. Tabuchi, A. Gloppe, K. Usami, and Y. Nakamura, *Appl. Phys. Express* **12**, 070101 (2019).
[20] E. Almpanis, *Optomagnonic Structures: Novel Architectures for Simultaneous Control of Light and Spin Waves* (World Scientific, Singapore, 2021).
[21] X. Zhang, C.-L. Zou, L. Jiang, and H. X. Tang, *Sci. Adv.* **2**, e1501286 (2016).
[22] C. Regal and K. Lehnert, *J. Phys.: Conf. Ser.* **264**, 012025 (2011).
[23] C. Zhong, X. Han, H. X. Tang, and L. Jiang, *Phys. Rev. A* **101**, 032345 (2020).
[24] Y.-S. Park and H. Wang, *Nat. Phys.* **5**, 489 (2009).
[25] M. Tomes and T. Carmon, *Phys. Rev. Lett.* **102**, 113601 (2009).
[26] A. B. Matsko, A. A. Savchenkov, V. S. Ilchenko, D. Seidel, and L. Maleki, *Phys. Rev. Lett.* **103**, 257403 (2009).
[27] G. Bahl, M. Tomes, F. Marquardt, and T. Carmon, *Nat. Phys.* **8**, 203 (2012).
[28] Y.-L. Zhang, C.-H. Dong, C.-L. Zou, X.-B. Zou, Y.-D. Wang, and G.-C. Guo, *Phys. Rev. A* **95**, 043815 (2017).
[29] J. A. Haigh, A. Nunnenkamp, A. J. Ramsay, and A. J. Ferguson, *Phys. Rev. Lett.* **117**, 133602 (2016).
[30] X. Zhang, N. Zhu, C.-L. Zou, and H. X. Tang, *Phys. Rev. Lett.* **117**, 123605 (2016).
[31] A. Osada, R. Hisatomi, A. Noguchi, Y. Tabuchi, R. Yamazaki, K. Usami, M. Sadgrove, R. Yalla, M. Nomura, and Y. Nakamura, *Phys. Rev. Lett.* **116**, 223601 (2016).
[32] S. Sharma, Y. M. Blanter, and G. E. W. Bauer, *Phys. Rev. B* **96**, 094412 (2017).
[33] G. Gantzounis, N. Papanikolaou, and N. Stefanou, *Phys. Rev. B* **84**, 104303 (2011).

- [34] T. Monteiro, J. Millen, G. Pender, F. Marquardt, D. Chang, and P. Barker, *New J. Phys.* **15**, 015001 (2013).
- [35] A. de los Ríos Sommer, N. Meyer, and R. Quidant, *Nat. Commun.* **12**, 276 (2021).
- [36] E. Almpanis, G. P. Zouros, P. A. Pantazopoulos, K. L. Tsakmakidis, N. Papanikolaou, and N. Stefanou, *Phys. Rev. B* **101**, 054412 (2020).
- [37] I. Stefanou, P. A. Pantazopoulos, and N. Stefanou, *J. Opt. Soc. Am. B* **38**, 407 (2021).
- [38] N. Stefanou, V. Yannopoulos, and A. Modinos, *Comput. Phys. Commun.* **132**, 189 (2000).
- [39] D. De Zutter, *IEEE Trans. Antennas Propag.* **30**, 898 (1982).
- [40] A FORTRAN computer code implementing the solution of the time-Floquet equations which appear in this paper can be found at <https://github.com/manolispan/BreathingSphere>.
- [41] E. Almpanis, N. Papanikolaou, and N. Stefanou, *Opt. Express* **22**, 31595 (2014).
- [42] Y. Liu, M. Davanço, V. Aksyuk, and K. Srinivasan, *Phys. Rev. Lett.* **110**, 223603 (2013).
- [43] T. Ojanen and K. Børkje, *Phys. Rev. A* **90**, 013824 (2014).
- [44] J. Kim, M. C. Kuzyk, K. Han, H. Wang, and G. Bahl, *Nat. Phys.* **11**, 275 (2015).
- [45] Y.-X. Zhang, S. Wu, Z.-B. Chen, and Y. Shikano, *Phys. Rev. A* **94**, 023823 (2016).
- [46] R. W. Peterson, T. P. Purdy, N. S. Kampel, R. W. Andrews, P.-L. Yu, K. W. Lehnert, and C. A. Regal, *Phys. Rev. Lett.* **116**, 063601 (2016).
- [47] D.-Y. Wang, C.-H. Bai, S. Liu, S. Zhang, and H.-F. Wang, *Phys. Rev. A* **98**, 023816 (2018).
- [48] M. Davanco, S. Ates, Y. Liu, and K. Srinivasan, *Appl. Phys. Lett.* **104**, 041101 (2014).
- [49] M. Rossi, N. Kralj, S. Zippilli, R. Natali, A. Borrielli, G. Pandraud, E. Serra, G. Di Giuseppe, and D. Vitali, *Phys. Rev. Lett.* **119**, 123603 (2017).
- [50] J. B. Clark, F. Lecocq, R. W. Simmonds, J. Aumentado, and J. D. Teufel, *Nature (London)* **541**, 191 (2017).
- [51] J. M. Dobrindt, I. Wilson-Rae, and T. J. Kippenberg, *Phys. Rev. Lett.* **101**, 263602 (2008).
- [52] S. Gröblacher, K. Hammerer, M. R. Vanner, and M. Aspelmeyer, *Nature (London)* **460**, 724 (2009).
- [53] F. Verhulst, *Nonlinear Differential Equations and Dynamical Systems* (Springer, Heidelberg, 2006).
- [54] G. Ptitcyn, A. Lamprianidis, T. Karamanos, M. Müller, R. Alaee, V. Asadchy, M. Mirmoosa, M. Albooyeh, S. Fan, C. Rockstuhl, and S. A. Tretyakov, in *Proceedings of the 2021 Fifteenth International Congress on Artificial Materials for Novel Wave Phenomena (Metamaterials)* (IEEE, Piscataway, NJ, 2021), pp. 347–349.
- [55] K. Schab, B. Shirley, and K. C. Kerby-Patel, in *Proceedings of the IEEE Transactions on Antennas and Propagation* (IEEE, Piscataway, NJ, 2022).
- [56] D. Mongin, V. Juvé, P. Maioli, A. Crut, N. Del Fatti, F. Vallée, A. Sánchez-Iglesias, I. Pastoriza-Santos, and L. M. Liz-Marzán, *Nano Lett.* **11**, 3016 (2011).
- [57] A. Toncelli, N. Capuj, B. Garrido, M. Sledzinska, C. M. Sotomayor-Torres, A. Tredicucci, and D. Navarro-Urrios, *J. Appl. Phys.* **122**, 053101 (2017).
- [58] D. Wright and R. Cobbold, *Smart Mater. Struct.* **19**, 045006 (2010).
- [59] R. Fleury, D. L. Sounas, and A. Alù, *Phys. Rev. B* **91**, 174306 (2015).
- [60] S. Noschese, L. Pasquini, and L. Reichel, *Numer. Lin. Alg. Appl.* **20**, 302 (2013).